Three-Dimensional Velocity Field Reconstruction

David Frakes
Mark Smith
Diane de Zélicourt
Kerem Pekkan
Ajit Yoganathan

Georgia Institute of Technology,
Atlanta, GA 30332

The problem of inter-slice magnetic resonance (MR) image reconstruction is encountered often in medical imaging applications. In such scenarios, there is a need to approximate information not captured in contiguously acquired MR images due to hardware sampling limitations. In the context of velocity field reconstruction, these data are required for visualization and computational analyses of flow fields to be effective. To provide more complete velocity information, a method has been developed for the reconstruction of flow fields based on adaptive control grid interpolation (ACGI). In this study, data for reconstruction were acquired via MRI from in vitro models of surgically corrected pediatric cardiac vasculatures. Reconstructed velocity fields showed strong qualitative agreement with those obtained via other acquisition techniques. Quantitatively, reconstruction was shown to produce data of comparable quality to accepted velocity data acquisition methods. Results indicate that ACGI-based velocity field reconstruction is capable of producing information suitable for a variety of applications demanding three-dimensional in vivo velocity data. [DOI: 10.1115/1.1824117]

1 Introduction

Flow within the cardiovascular system has historically received much attention in the field of biomedical engineering due to the paramount importance of cardiovascular function in sustaining life. A greater understanding of cardiovascular flow conditions has been provided by many previous studies [1–4]. Such studies depend on the acquisition of high-quality in vivo data for success.

Limitations associated with the acquisition of in vivo velocity data have hindered efforts to effectively analyze blood flow in the past. Previously, most analyses of in vivo conditions have required invasive procedures such as catheterization to obtain velocity and pressure measurements. These procedures expose patients to high levels of risk and discomfort. Accordingly, the development of noninvasive methods to acquire in vivo flow data is desirable. Previous efforts aimed at reconstructing velocity fields from MR data have addressed the problem with limited success. Most inter-slice MR reconstruction schemes are suited to handle morphological data rather than velocity information [5–11]. Here, a novel approach based on adaptive control grid interpolation (ACGI) is presented for the reconstruction of velocity fields from MR images.

2 Background

2.1 Motivation. The surgical treatment of single ventricle congenital heart defects (CHD's) in children is one area in which fluid flow analyses have made a significant contribution. The problem is frequently observed, affecting two newborns out of every thousand [12]. Congenital Heart Defects are treated palliatively with the total cavopulmonary connection (TCPC), one variety of the Fontan operation. This operation allows the atypical heart found in these children to function more effectively. Children with single ventricle anatomies have a mixing of oxygenated and deoxygenated blood, which when left untreated leads to numerous problems. A simplified depiction of the communication between the right and left heart that facilitates mixing is illustrated in Fig. 1(*a*). The TCPC procedure results in a complete bypass of the right heart with the single ventricle driving blood through the entire circulatory system. The resultant anatomy is characterized by a reconnection of the pulmonary arteries (PAs) to both the superior vena cava (SVC) and inferior vena cava (IVC), which have been detached from the right atrium (RA). An illustration of the modified anatomy is shown in Fig. 1(*b*).

Much of the power produced by the single ventricle pump is consumed in systemic circulation. Accordingly, minimizing power loss in the modified vasculature is imperative for successful results. It is within this framework that an effective analysis of fluid flow within the TCPC becomes extremely valuable as it can provide the information necessary to evaluate power loss. Furthermore, this information can be used to correlate efficient flows with specific anatomical characteristics imparted to the modified anatomy. This in turn can provide surgeons with fundamental goals to pursue in executing future operations that when achieved facilitate successful surgical outcomes.

Historically, the surgeon's experience has been the primary factor in determining surgical design with little attention paid to fluid dynamics. In order to focus connection design on minimizing power loss, surgical evaluation tools are under development at the Georgia Tech Cardiovascular Fluid Dynamics Laboratory. These tools will aid the surgeon in creating efficient vascular structures that contribute to longer and higher quality lives for patients.

2.2 Power Loss Estimation. One method of evaluating the efficiency of fluid flow is via power loss estimation. Simply put, if flow through a given morphology is efficient, little power is dissipated. In the context of the Fontan, a direct relationship has been observed between inefficient flow and poor surgical outcomes. For this reason, the prospect of quantifying power loss in vivo, in order to identify advantageous anatomical characteristics, is attractive. The question is thus posed, how can power loss be estimated in vivo? The answer depends on the inputs available for power loss to be calculated.

One technique that has been used extensively in power loss quantification is control volume analysis. In order to execute control volume analysis, both pressure and velocity data are required as described by Eq. (1).

$$\dot{E}_{Loss} = -\oint_{CS}\oint\oint \left[p + \frac{1}{2}\rho u_i u_i\right] u_j n_j dS \tag{1}$$

Here p represents pressure, ρ represents density, the u variables represent respective components of velocity, and n represents a normal vector. The subscripts with each vector variable indicate Einstein notation. Obtaining the data required to satisfy this equa-

Contributed by the Bioengineering Division for publication in the JOURNAL OF BIOMECHANICAL ENGINEERING. Manuscript received July 23, 2003; revised manuscript received July 13, 2004. Associate Editor: C. Ross Ethier.

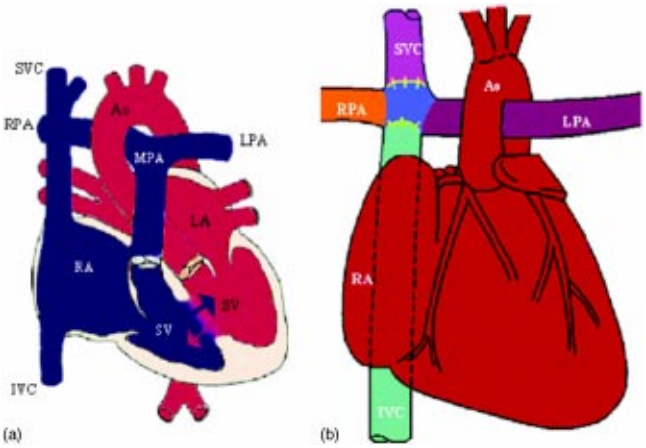

Fig. 1 Illustration of a human heart with a single ventricle CHD (*a*). The communication between the two ventricles indicated by the arrows facilitates the mixing of oxygenated and deoxygenated blood. The anatomical modification performed to palliate this condition, the TCPC, is shown in (*b*).

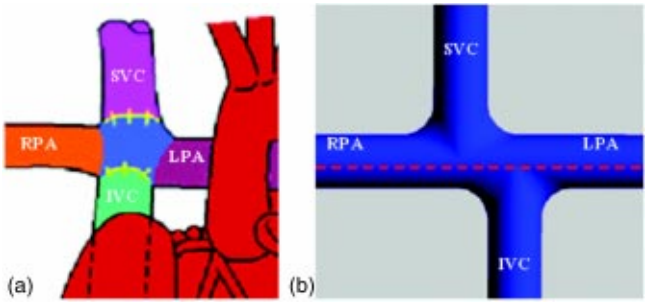

Fig. 2 Illustrations of the TCPC configuration (*a*) and the phantom geometry (*b*) used to simulate it. The dashed line in (b) is present for a later discussion.

tion can be problematic in vivo in that pressure information is difficult to extract. For cardiovascular cases, pressure data is usually gathered via catheterization, which is highly invasive and subjects the patient to risk and discomfort. Alternatives to catheterization are desirable primarily for these reasons and because of the 20% error margin generally associated with the process.

One alternative for generating pressure data is computational fluid dynamics (CFD) simulation [13]. The inputs required for CFD are a geometric structure and boundary conditions for that structure in the form of velocity profiles. A completed CFD simulation yields detailed pressure and velocity data throughout the specified geometry. Control volume analysis can be used following CFD simulation to estimate power loss. With respect to the surgical evaluation scenario, geometric structures can be derived from MR imaging followed by morphological reconstruction. Accordingly, this mechanism for estimating power loss can be applied to address the problem described in Section 2.1. However, such power loss estimates are based on simulated velocity and pressure data, one step removed from real in vivo data like that used to derive the geometric input and boundary conditions for CFD. Implementation of this process has been successful for numerous researchers, but from a theoretical standpoint power loss quantification based directly on in vivo data would be preferred [14,15].

Another method for estimating power loss that has been explored more recently makes use of the viscous dissipation function [16]. Here, local fluid power losses produced by viscous dissipation are computed based on velocity gradients. Although these values are generally small in the local sense, the total power loss can be calculated as the integral of the dissipation function over the selected volume of interest. Expressions for the dissipation function and associated fluid dynamic power losses are described by Eqs. (2) and (3), respectively.

$$\Phi = \frac{1}{2}\left(\frac{\partial u_i}{\partial x_j} + \frac{\partial u_j}{\partial x_i}\right)^2 \tag{2}$$

$$\dot{E}_{Loss} = \mu \int_{CV}\int\int \Phi \, dV \tag{3}$$

In these equations, Φ is the dissipation function, u represents velocity as before, and x is used to represent Cartesian directions. Subscripts in the first equation again indicate Einstein notation. CV represents the control volume over which power loss calculations are performed, and dV represents the differential volume element within the control volume. Equations (2) and (3) reveal the important fact that the viscous dissipation function can be calculated with velocity gradients alone. For this reason a purely velocity-based pathway for accomplishing power loss estimation is possible with respect to clinical medicine. All of the power loss quantification methodologies discussed thus far have been derived and covered more extensively in a recent publication [16].

Accurately quantifying power loss via the viscous dissipation function requires the measurement of all three velocity components in all three spatial dimensions. Furthermore such data must be sufficiently resolved near the boundaries of flow where velocity gradient magnitudes are high. Ultrasound has proven valuable in a variety of velocity imaging scenarios, but fundamental limitations associated with the modality prohibit the acquisition of all three components of velocity and make it poorly suited for this application. Phase-encoded MR velocity images provide high-resolution velocity information, but only in two spatial dimensions. In order to use this information for viscous dissipation function power loss quantification, reconstruction into three dimensions is demanded. Toward this end, a method to reconstruct MRI velocity data has been developed so that the reconstructed data can then be used to estimate power loss with the viscous dissipation function.

2.3 Initial Results. Previous studies by Healy et al. and Sharma et al. have provided results pertaining to the accuracy of the dissipation function with respect to alternatives [16,17]. Specifically, control volume analysis following CFD simulation was compared to viscous dissipation function analysis using the same CFD simulated data. These results were insightful as they displayed the capability of the dissipation function by comparing results from the two methods based on a common data source.

To relate the two power loss estimation techniques to the Fontan scenario, the Sharma et al. and Healy et al. studies employed a phantom TCPC connection. The phantom geometry is displayed in Fig. 2 where the TCPC configuration from Fig. 1(*b*) is revisited for comparison. The TCPC configuration displayed in Fig. 2(*a*) is an artist's rendition of the anatomy that shows an idealized connection lacking some of the subtleties of the most popular current implementation. The phantom shown in Fig. 2(b) was designed to include these subtleties, specifically connection site flaring and caval offset, in order to better simulate the in vivo conditions that are most common today.

A variety of flow splits and cardiac outputs were simulated to compare the power loss estimation techniques under different conditions. Flow splits here are described as the percentage of the total flow departing the model from the LPA and RPA conduits, while total cardiac output (TCO) represents the total flow entering both the IVC and SVC conduits. Total cardiac output and total flow rate are used interchangeably in this text. For all experiments in the Healy et al. and Sharma et al. studies, the IVC/SVC flow split was held constant at 60/40 for a total cardiac output of 2 L/min. These values and LPA/RPA flow split values were based

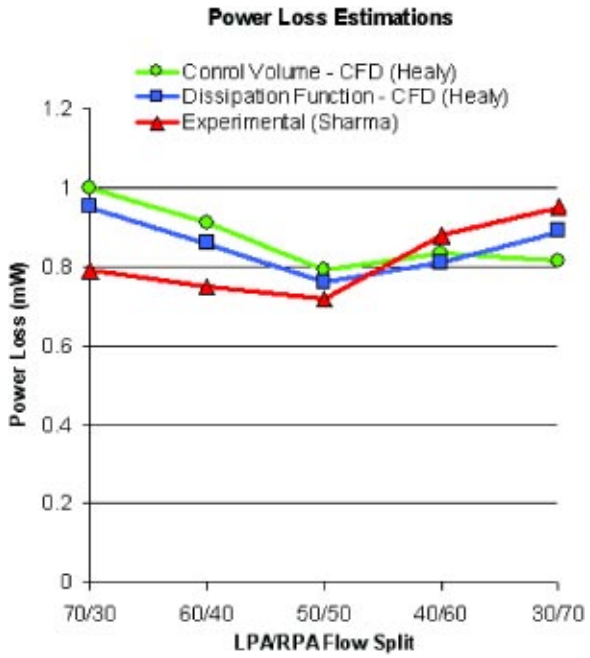

Fig. 3 Results from different power loss estimation techniques. Control volume analysis and viscous dissipation function analysis show strong agreement for all flow splits.

on in vivo MR velocity measurements from pediatric CHD patients under resting conditions. In addition to control volume analysis and dissipation function analysis, power losses were also calculated in the Sharma et al. study based on direct measurements from an in vitro phantom with the same geometric properties as the CFD model. These experimental power loss values were calculated based on IVC, SVC, LPA, and RPA pressures measured using high fidelity pressure transducers and on inlet and outlet flow rates measured with rotometers [17,18]. The results from all three power loss analyses conducted in the Healy et al. and Sharma et al. studies are displayed in Fig. 3.

Power loss values estimated with control volume analysis and the viscous dissipation function showed strong agreement over the entire range of LPA/RPA flow splits explored. The errors between these two approaches were less than 10% in all cases, ranging from 3.2% to 9.9%. Differences between the results from both of these methods and the experimental results were likely caused by poorly regulated boundary conditions in the Sharma et al. study. However, these results indicate that, based on the same data, the viscous dissipation function is capable of providing power loss estimations with accuracy comparable to control volume analysis. In the context of using reconstructed velocity fields to quantify power loss, one more question remains. Specifically, it has not previously been shown that reconstruction can generate velocity data with sufficient accuracy to estimate power loss well. The validations in Section 3 are aimed at addressing this point.

3 Methods

3.1 Data Acquisition. A flow loop similar to that used by Sharma et al. was constructed to circulate fluid through the TCPC phantom under steady flow conditions. A blood analog fluid composed of water and glycerine with a viscosity of 3.5 cP and a density of 1.1 g/cm^3 was used. Entrance lengths sufficient to ensure fully developed flows were connected to the phantom inlets. Total flow rates of 2 and 4 L/min were explored for a constant IVC/SVC flow split of 60/40 and LPA/RPA flow splits ranging from 40/60 to 60/40 in 10% increments. A contiguous set of phase-encoded velocity images were acquired as the initial step of the reconstruction process presented here. MRI data for this work were acquired using a Philips 1.5 Tesla Gyroscan scanner. Specific parameters relating to data acquisition are given in Table 1.

Table 1 Parameters associated with MR data acquisition

MR system type	Philips
Pulse sequence type	Gradient echo
Acquisition plane	Transverse
Images acquired	~15
Slice thickness	5 mm
Field of view	200 mm×200 mm
Flip angle	35°
Repetition time	23 ms
Echo time	6.2 ms
Averaged signals	2
Matrix size	256×256
VENC	70 cm/s

3.2 Data Reconstruction. To reconstruct velocity fields as a precursor to power loss estimation, a new reconstruction methodology has been developed based on adaptive control grid interpolation (ACGI). ACGI has previously been employed in addressing video coding and tracking problems, as well as data reconstruction [19]. The extension of the technique to reconstructing velocity data is a new concept. ACGI is a hybrid motion estimation scheme that has features of both block-based and optical flow-based methods. These techniques, previously developed for frame prediction in movies and camera video, provide a foundation for MRI reconstruction algorithms. For the purpose of context and perspective, this section provides a brief overview of motion estimation.

3.2.1 Motion Estimation. The goal of ACGI, and any other motion estimation scheme for that matter, is to link the pixels from a pair of images such that when the differences between all pairs of linked pixels are summed, a minimum value results. This collective difference is more easily conceptualized considering a matrix of vectors pointing every pixel in one image to a corresponding location in a second image. For each pixel, there is some difference between its intensity and the intensity at the corresponding location in the second image. The summation of these differences, for a pair of images and a corresponding motion field, yields insight into how well that motion field links the image pair. This ''image difference'' quantity can be determined based on several traditional formulations; here a squared error measure, referenced later as Eq. (5), is employed. The ''image difference'' in general will be referred to throughout this section in defining the new methodology.

Two conventional methods of estimating motion are block matching and optical flow. Both techniques describe the movement of pixels from one image frame to another. Although they address the same problem, these two methods approach it from very different perspectives.

Block matching in its simplest form consists of comparison and search steps. Blocks of pixels from one image are compared to blocks from a second image to determine the region in that second image most similar to the chosen region in the first. Here again the goal is to minimize the image difference defined earlier. The displacement of all pixels within a block is governed by a single motion model, the simplest and most common example being uniform displacement. The similarity between blocks is evaluated via an error function that quantifies the image difference, or collective intensity discrepancy, between two regions. In the search step, allowable model parameters are searched to find optimal values [19]. Block-based approaches have the advantage of a compact pixel displacement representation and a simple search procedure for simple models. These search techniques become computationally expensive when the model order, and consequently the search

space, are increased. These increases are likely to be required when complex motion is present and high-accuracy estimates are needed.

The other conventional approach is optical flow, which allows each pixel to follow a unique path from frame to frame. The flexibility of this technique leads to a less compact motion field representation and requires more computation. Unlike the simpler block matching approach where motion is estimated for entire local neighborhoods, optical flow determines a unique motion for every pixel. This is accomplished by satisfying the optical flow constraint equation (OFCE),

$$\frac{\partial I(x,y,t)}{\partial x}\frac{\partial x^*(t)}{\partial t}+\frac{\partial I(x,y,t)}{\partial y}\frac{\partial y^*(t)}{\partial t}+\frac{\partial I(x,y,t)}{\partial t}=0 \quad (4)$$

where $I(x,y,t)$ represents the intensity function for a given image, and $x^*(t)$ and $y^*(t)$ denote the true trajectory of each point [20]. A unique solution to Eq. (4) is found by assuming motion field smoothness, a constraint which is imposed in conjunction with minimizing the OFCE error. The OFCE error, or its difference from zero, provides another measure of the previously defined image difference. Imposing the smoothness constraint is justified in the context of this work because it is consistent with the smooth variations of flow morphologies obtained when data sets are acquired with contiguous MR slices.

The concept of motion estimation relates well to inter-slice reconstruction when fluid structures at different positions in different MR slices are considered as objects moving from frame to frame. That is to say, similar flow features are viewed mathematically as a single structure undergoing motion. With respect to applying optical flow, the transition from one image plane to either adjacent one can be considered analogous to the transition from time t to time $t+1$ in a temporal image sequence.

3.2.2 The New Approach. The limitations associated with traditional approaches motivate the combination of block and optical flow-based methods into a superior hybrid. The ACGI approach used in this work can be considered both block-based and optical flow-based. ACGI estimates displacement with an iterative search based on the optical flow equation, but the image is partitioned into regions as in the block-based approach.

The execution of ACGI begins with an initial image partitioning. A quad-tree grid structure is used to divide an image first into four regions of equal size, then into sub-regions as necessary. Following the initial partitioning, motion fields for each of the four sub-regions of the image are determined. Each motion field is defined based on the motion vectors associated with the corners of the region, which are referred to as control points. Specifically, the motion vector for any point on the interior of a sub-region is related to the four control points that bound it via bilinear interpolation. Given this relationship, the motion field for an entire region can be defined based on four parameters, those being the displacement vectors associated with each of the four control points.

The process used to derive the motion field varies these four parameters iteratively in order to minimize the error associated with the OFCE for a given block. A conjugate gradient method is employed to optimize the motion field efficiently. Within this optimization framework, the constraint is motion field smoothness, imposed as in the optical flow solution defined earlier, and the expression to be minimized is the error function, defined explicitly for a region R as,

$$E(\bar{\alpha},\bar{\beta})=\sum_{\mathbf{n}\in R}\sum (I[\mathbf{n},k]-I[n_1+\bar{\alpha}^T\bar{\theta}(\mathbf{n}),n_2+\bar{\beta}^T\bar{\phi}(\mathbf{n}),k+\delta k])^2 \quad (5)$$

In this expression, $\bar{\alpha}$ and $\bar{\beta}$ represent vectors composed of the respective row and column components of the control point displacements, $I[\mathbf{n},k]$ represents an image where the vector $\mathbf{n}=(n_1,n_2)$ denotes coordinates within that image, and $\bar{\theta}$ and $\bar{\phi}$ represent basis functions that implement the bilinear interpolation mentioned earlier. Relating this expression to the previous conceptual discussion, the summation corresponds to the image difference between one image and the motion corrected version of another. Here it is clear that this quantity can be minimized based on the control point vectors ($\bar{\alpha}$ and $\bar{\beta}$) given that the basis functions $\bar{\theta}$ and $\bar{\phi}$ are explicitly defined. In summary, the process for determining the motion field for each region is characterized by the block diagram shown in Fig. 4.

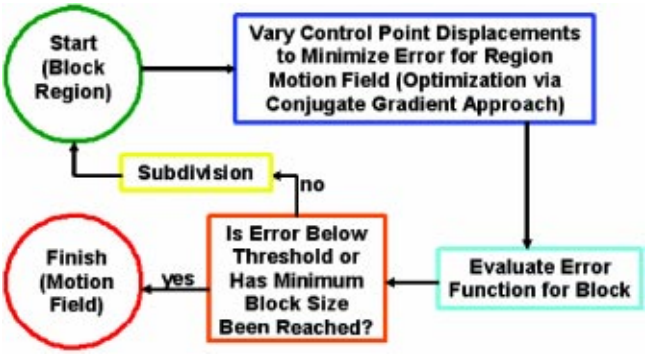

Fig. 4 Block diagram illustrating the ACGI motion field derivation process

Several other characteristics of the resultant motion field are noteworthy. Because this motion model is of the connected variety, the displacements for a given region's control points are the same for each of those control points with respect to other regions that they bound. This makes the motion field continuous as a whole. So for the entire image, the ACGI motion vector field is guaranteed to be piecewise smooth and globally continuous.

In terms of reconstructing fluid flow well, global continuity is especially significant because it guarantees that the motions for all regions are linked and that no local estimation is carried out independently of the motion information pertaining to adjacent regions. This characteristic allows the algorithm to perform acceptably in the case that a fluid structure is present in one slice then gone in the next. The problem of estimating motion is ill-posed in this scenario, but assuming that the majority of the image is composed of features that span the image pair, the solutions in the well-posed regions will dominate and shape the results in the poorly conditioned area. Under these circumstances, and for all cases truly speaking, a perfect solution is unattainable, but a best solution given constraints is still achieved. For this best solution to be of useful quality, sampling must take place at a sufficiently fine rate. Given the results presented here, slices 5 mm thick appear to fall below the upper bound on slice thickness corresponding to the minimum acceptable spatial sampling rate.

The quad-tree grid structure generated via the adaptive process used here can take many forms. One example of a course symmetric quad-tree, superimposed on an image from the pair used to generate it, is shown in Fig. 5. The image here is a modulus image from the velocity scan, indicating signal strength, and corresponds to the plane indicated by the dashed red line in Fig. 2(*b*). Images of this type are well-suited to establish appropriate interpolation vectors as the image intensity is a function of fluid moving in and out of the imaging plane. Accordingly, the criteria for vector determination are based, at least in part, on all three velocity components to be reconstructed. By exploiting this information similar fluid structures can be correlated well via the ACGI methodology.

In Fig. 5 the blue lines represent the initial image partitioning, and the green and red lines define sub-regions where grid refinement is advantageous. When further subdivision is not performed in these regions, the bilinear model approximates motion poorly. Successive refinement decreases the area that the model is im-

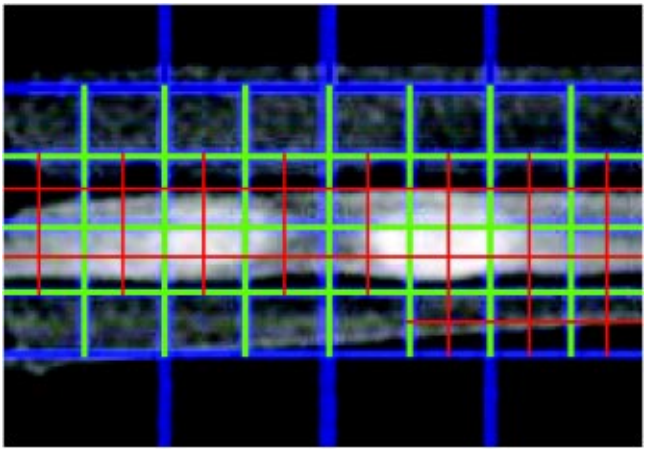

Fig. 5 Example of a coarse symmetric quad-tree structure generated via the ACGI motion estimation process

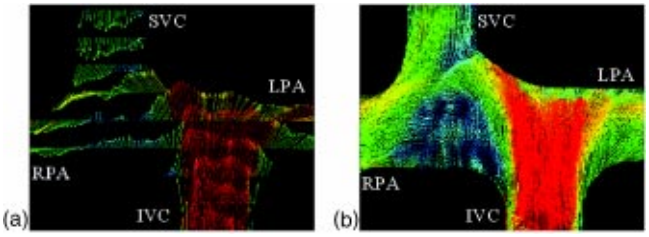

Fig. 6 Coronal view of an originally acquired phase encoded MRI velocity data set (*a*) and the same view of the corresponding three-dimensional velocity field reconstruction (*b*)

posed over in each partition and decreases overall error significantly. As this figure indicates, the most subdivided regions of the image correspond to areas of the phantom within which fluid is flowing and high motion field resolution is desired to facilitate accurate reconstruction. Progressive subdivision, like the motion parameter determination phase itself, is performed based on the image difference value. When successive subdivision and the associated motion field refinement are not accompanied by a sufficient decrease in the image difference, a further subdivision is foregone. This was determined to be the case in practice when a subdivision produced less than a 5% decrease in error. These mechanics partition the image into sub-blocks of appropriate size to capture characteristics of transition and further subdivide regions where error remains large. They enable the algorithm to handle both simple and complex displacements within the optical flow framework. These characteristics are important as they allow us to obtain an accurate and dense representation of the displacement field at a reasonable computational cost. There is a tradeoff between the computation time and the error associated with the resultant displacement field when the block size bounded by control points is varied. Smaller block sizes lead to a more accurate displacement field, but are more computationally expensive. If large errors remain, a further subdivision is performed to improve the resolution of the motion field. Ultimately, the motion field can be calculated with a specified degree of sub-pixel accuracy. In order to maximize efficiency, subdivision and the accompanying computation are confined to regions where nonuniform motion is present as in Fig. 5. Further details describing the characteristics of the motion model implemented here can be found in a recent publication [21].

3.2.3 Algorithm Description. The starting point for the overall reconstruction process is a set of transverse contiguous phase-encoded MR velocity images acquired with a breath-hold gradient echo pulse sequence as described in Section 3.1. Phase velocity mapping has been explored extensively in other research and established as an accurate means of extracting flow data [22]. Fields of displacement vectors are calculated describing the motion of pixels from one image slice to another via the ACGI methodology outlined in the previous section.

From a dense displacement field and the associated pair of MR images, intermediate frames are reconstructed. By following one of the displacement vectors a portion of the way from one slice to the next, a linear approximation of where a given pixel would be found in an intermediate slice can be made. Repeating this process for all pixels in a given slice allows the reconstruction of an entire intermediate image. Pairs of these reconstructed images are then combined in a spatially weighted sum to form a single interpolated slice. This process is repeated and multiple interpolated images are stacked between known images to produce a three-dimensional enhanced data set. The out-of-plane spatial resolution of the enhanced data is determined by the number of interpolated frames, and can be varied although it is generally advantageous to achieve an out-of-plane resolution close to the in-plane value associated with the originally acquired data. Adding interpolated frames beyond this point is analogous to computing a value with greater precision than the inputs it is based on, and offers no further benefit.

4 Results

The improvement produced by ACGI in comparison to an original MR data set is displayed in Fig. 6. Here the sparse originally sampled data is displayed in (*a*) and the reconstructed velocity data set in (*b*). The total cardiac output for these data was 4 L/min, the IVC/SVC flow split was 60/40, and the LPA/RPA flow split was 40/60.

The immediate focus of the validations associated with this work was to demonstrate the accuracy of reconstructed data. The accuracy of the dissipation function for power loss estimation based on velocity data from other sources has already been explored and was described by the data provided in Sec. II. Accordingly, the important question to answer in the context of using reconstructed data to estimate power loss relates directly to the accuracy of those data. However, the ultimate aim of research along these lines is to use reconstructed MR data to quantify power loss. For this reason, initial results obtained by applying the viscous dissipation function to these data are included in this section as well.

In order to evaluate the quality of reconstructed velocity data, reconstructions were compared to velocity planes from identical locations in the same phantom acquired with particle image velocimetry (PIV) and computational fluid dynamics (CFD). PIV and CFD methodologies have been extensively explored by previous research [23,24]. Planes for comparison were taken from the coronal perspective, out-of-plane with respect to the original MR scan. The coronal planes reconstructed from MR contain almost exclusively reconstructed data since the images used to derive them were taken from the axial perspective. Accordingly, the comparison of these reconstructed planes to ones natively acquired in the coronal perspective with other modalities offers valuable insight into the quality of reconstruction.

Although there is no absolute gold standard for correct velocity data, fluid physics dictate that the divergence of any velocity field must equal zero,

$$\frac{du}{dx}+\frac{dv}{dy}+\frac{dw}{dz}=0 \tag{6}$$

where u, v, and w represent the three orthogonal components of velocity and x, y, and z again represent Cartesian directions. To demonstrate that the data reconstructed with the proposed algorithm are realistic, divergence errors for the symmetry plane of the TCPC phantom were calculated for the most common set of in

Table 2 Results from divergence error analysis

Data set	RMS divergence error
CFD	2.9
PIV	14.4
ACGI reconstructed MRI	17.6
Cubic interpolated MRI	19.4
Raw MRI	57.1

vivo flow conditions: the total cardiac output 2 L/min, IVC/SVC flow split 60/40, and LPA/RPA flow split 50/50. The root mean square divergence error values were evaluated for five different data sources: CFD, PIV, ACGI reconstructed MRI, cubic interpolated MRI, and raw MRI. The L2 norms of divergence error values varied greatly in some cases because differing numbers of points were examined, but the root mean square values,

$$\mathrm{RMS} = \sqrt{\frac{\sum_{i \in D} (E_i)^2}{n}} \tag{7}$$

offered greater comparative insight. In Eq. (7), E_i denotes the individual divergence errors, their difference from zero, D represents the fluid domain, and n represents the number of points over which the divergence errors were summed. Divergence values have the unit $1/s$, which interestingly is also the unit associated with the OFCE once variables have been transformed to match those of the data it is applied to in this scenario. The results of the divergence error calculations are presented in Table 2.

The divergence errors associated with CFD were expected to be small, as upholding divergence is one of the criteria used to determine the solution within the framework of CFD. Furthermore, the greater levels of noise present in the reconstructed MRI data were expected to contribute to errors in divergence. Nevertheless, the divergence errors for the ACGI-reconstructed MRI data were well within an order of magnitude with respect to the RMS value. The number of points examined for the ACGI-reconstructed MRI and PIV data sources were approximately equal. Although the ACGI-reconstructed MRI data showed greater divergence errors than PIV, the proximity of those errors to the corresponding values from PIV is encouraging as the PVI data were actually acquired in the plane that was analyzed, whereas 87.5% of the data in the reconstructed MRI plane were interpolated values. ACGI-based MRI reconstruction showed an enormous improvement over the raw MRI data with respect to divergence, and a significant improvement, 10.23%, over cubic interpolation. The infinity norm of the ACGI-reconstructed data was also better than that associated with cubic interpolated data by greater than 10%. In the ongoing effort to enable reconstructions of the highest quality, one algorithmic development underway involves the incorporation of a divergence term in the error expression that is minimized to determine the optimal motion field. This should facilitate the reconstruction of data characterized by even lesser divergence errors.

In a second data comparison, velocity magnitudes were evaluated on a point-by-point basis. This comparison reflects the accuracy of data in a different way as there are an infinite number of zero-divergence velocity fields that can occupy a volume, but clearly only one of them is correct for this flow phantom and the given inputs. Intensity values representing the magnitude of velocity at each pixel location were compared between MR reconstruction and both PIV and CFD. The magnitudes of the differences between these values were then summed for all pixel locations and averaged. PIV and CFD were compared as well. The goal of this analysis was to evaluate ACGI reconstruction with respect to an established acquisition technique and an established simulation technique. Including the raw MRI data in this analysis would be inappropriate as the large gaps between the original slices make coronal planes incomplete. Cubic interpolated data were also omitted from this comparison as visual inspection clearly demonstrates that they are distorted (Fig. 9). The error evaluation methodology employed in this stage is frequently used for image-based comparisons, and was selected here as there were two images, each from a different modality, to be compared in every case [25]. Details describing the CFD and PIV methodologies can be found in recent publications from the Georgia Tech Cardiovascular Fluid Mechanics Laboratory [16,23].

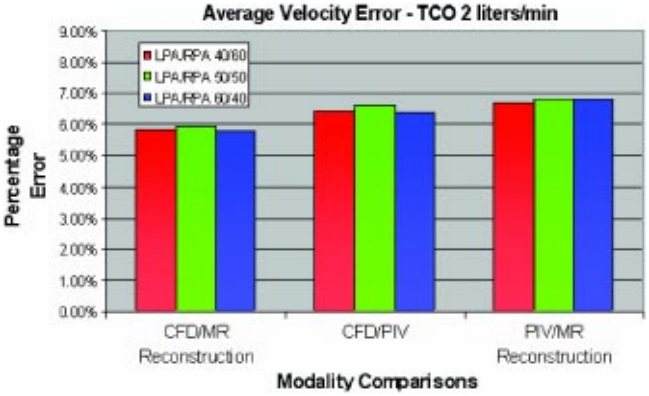

Fig. 7 Comparative errors for velocity magnitude acquisitions at a total cardiac output of 2 L/min. The values indicate the percentage formed by dividing the average error for each modality comparison by the theoretical maximum flow velocity within the phantom.

A variety of flow conditions similar to those explored by Healy et al. and Sharma et al. were examined to validate the effectiveness of ACGI reconstruction under different circumstances. LPA/RPA flow splits ranging from 40/60 to 60/40 were explored for both 2 and 4 L/min. This set of flow parameters covers the range encountered in vivo under normal and exercise conditions for pediatric CHD patients. Results from the error comparisons associated with each set of flow parameters are displayed in Figs. 7 and 8. To provide perspective, the errors are represented as a percentage relating the modality specific scaled velocity error to a common flow velocity. The average velocity discrepancy for each image pair was compared to the theoretical maximum velocity present within the model to determine the percentage. The maximum value was derived by dividing the largest entering flow rate by the cross-sectional area of the model inlet, to obtain an average value, and then multiplying by two to get the theoretical maxi-

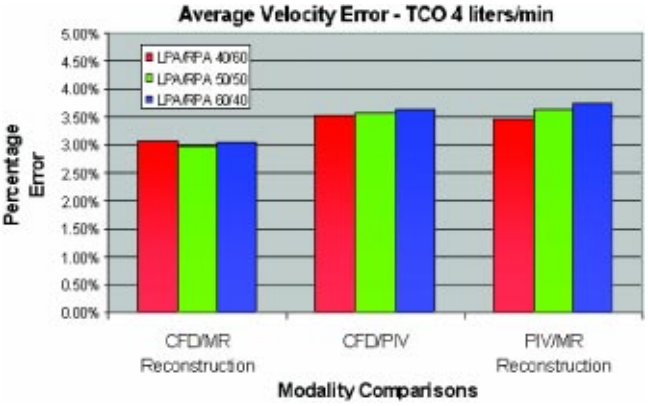

Fig. 8 Comparative errors for velocity magnitude acquisitions at a total cardiac output of 4 L/min. The values indicate the percentage formed by dividing the average error for each modality comparison by the theoretical maximum flow velocity within the phantom.

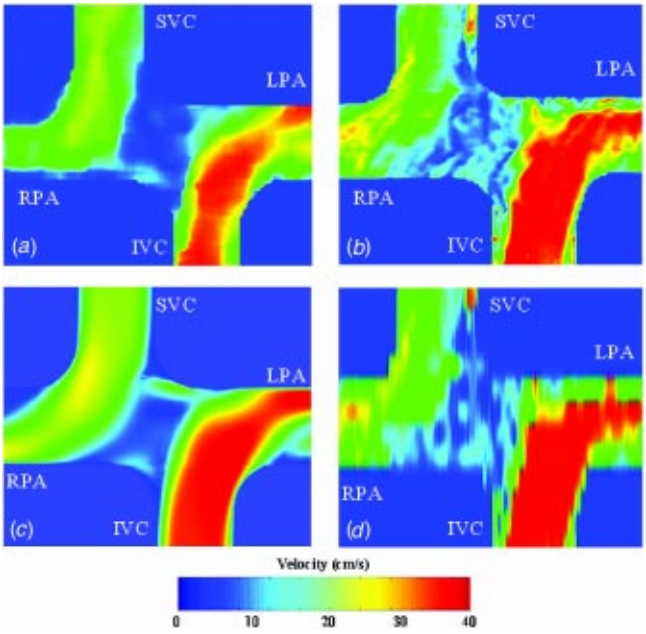

Fig. 9 (*a*) PIV, (*b*) MR reconstruction, (*c*) CFD, and (*d*) MR (bicubic interpolation) velocity magnitude contour plots. TCO: 4 L/min, IVC/SVC flow split: 60/40, LPA/RPA flow split: 60/40.

mum velocity present at the given flow rate under the assumption of parabolic flow. For 2 liters/min the theoretical maximum velocity in this model was 30.14 cm/s; for 4 liters/min it was 60.27 cm/s.

The similarity between reconstructed velocity planes and those from CFD and PIV can be observed directly from the data as well. Velocity magnitude plots for PIV, MR reconstruction, CFD, and bicubically interpolated MR data are displayed in Fig. 9. Bicubic interpolation is currently the most popular technique used to counteract sparse sampling in multi-planar reconstruction applications [26].

In Fig. 10, velocity vector plots for the same flow conditions are shown for all three modalities. For these data the total cardiac

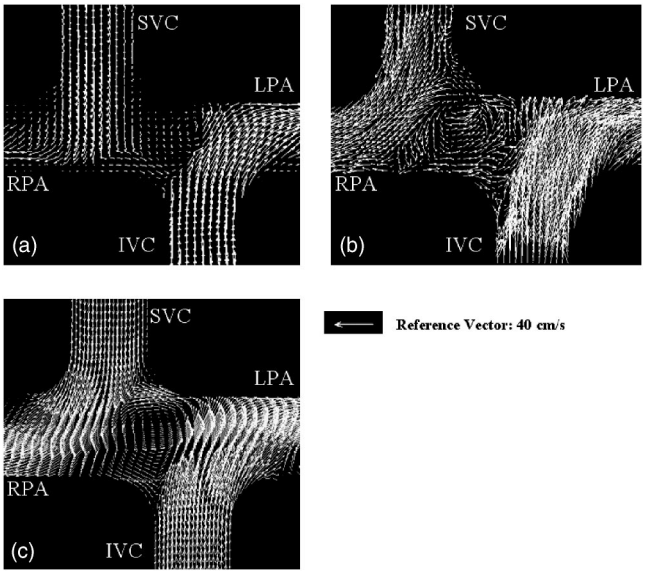

Fig. 10 (*a*) PIV, (*b*) MRI reconstruction, and (*c*) CFD velocity vector plots. TCO: 4 L/min, IVC/SVC flow split: 60/40, LPA/RPA flow split: 60/40.

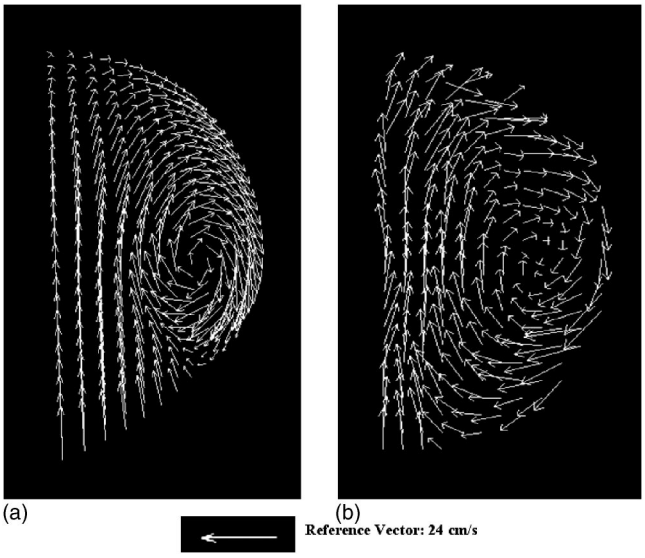

Fig. 11 (*a*) CFD and (*b*) MRI reconstruction LPA cross-section half-plane velocity vector plots. TCO: 2 L/min, IVC/SVC flow split: 60/40, LPA/RPA flow split: 50/50.

output was 4 L/min, the IVC/SVC flow split was 60/40, and the LPA/RPA flow split was 60/40. The results in Fig. 8 are consistent with the vector plot in Fig. 10, where it appears that SVC flow is more vertically aligned for PIV in comparison to CFD and MRI, which show SVC flow tending more toward the RPA. The CFD and MRI plots also show connection region vorticity and flow redirection from the IVC to the RPA, characteristics which are absent from, or less prevalent in, the PIV representation.

Reconstructed velocity data in the sagital plane corresponded well to those from CFD also. Figure 11 shows half-planes from CFD and reconstructed MR data just outside the connection region of the TCPC model. PIV data from this plane was unavailable due to limitations associated with the modality. It is noteworthy that the original MR data set contained only four axial image samples through the region of the model shown here, which account for only four horizontal lines of vectors in these illustrations.

When comparing reconstructed MRI data to MRI data natively acquired in the coronal plane, similar fluid structures were again observed. Figure 12 shows vector plots from a coronal MRI image and from reconstructed MRI data. Originally acquired MRI data and PIV data were included in this study for thoroughness, but the authors feel that the similarities between reconstructed MRI and

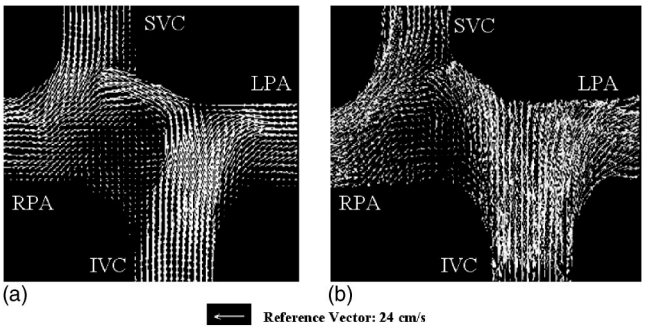

Fig. 12 Originally acquired coronal MRI data (*a*) and the corresponding coronal plane from the reconstructed MRI data set (*b*). Similar fluid structures including redirection of IVC flow to the RPA and the low-velocity offset region are apparent. TCO: 2 L/min, IVC/SVC flow split: 60/40, LPA/RPA flow split: 40/60.

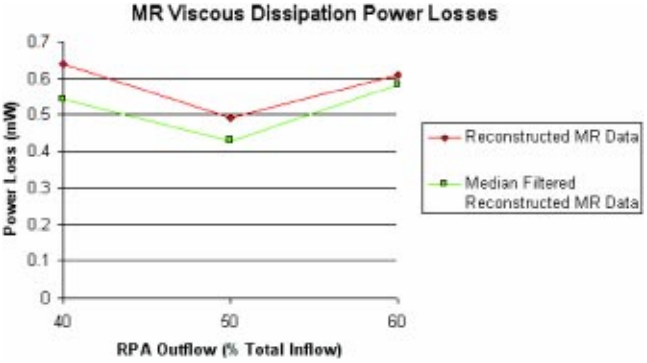

Fig. 13 Initial viscous dissipation power loss results for center planes based on reconstructed MR data at a total cardiac output of 2 L/min.

CFD data are most telling, as these are the only two data sources that provide all three components of velocity in three spatial dimensions.

Initial power loss figures obtained by applying the viscous dissipation function to reconstructed MR velocity planes showed similar trends to the power losses calculated in the Sharma et al. and Healy et al. studies for the same in vitro phantom. Specifically, a minimum power loss value was observed at an LPA/RPA flow split of 50/50. Increased power losses were observed when the flow split was varied in either direction. The power loss values for the center planes examined by the error comparisons in this section are displayed in Fig. 13.

As with any calculation based on acquired data, the accuracy of power loss figures here is directly related to the quality of the originally acquired MR information. One issue inherent to reconstructed MR velocity data, in contrast to the other velocity data acquisition modalities, is the relatively high level of noise in the original MR images. Figures 9 and 10 show clearly that the reconstructed MR data are much noisier than either CFD or PIV data. The noise in the reconstructed data, resulting from noise in the original images, can be alleviated by applying a median filter. Using a 3×3 median filter resulted in decreased viscous dissipation power losses. These median filtered power loss values are included in Fig. 13. Median filtering is not presented here as a recommended path for arriving at more accurate power loss values, as it certainly blurs the information near the boundaries that is imperative for accurate power loss measures. Rather, it is presented to support that noise is a factor with the MR data. It is probable that this noise contributes to the greater than expected power loss values for the center planes when compared to the global power losses presented by Sharma et al. and Healy et al. Because noise in the original data is a likely cause for the reconstruction-based power losses being overestimated, it is reasonable to conclude that the techniques presented here will be able to provide even higher-quality results as MR technology advances.

For the plane-to-plane comparisons conducted here to be significant, it is clear that planes used in comparison must have originated from the same locations within the model. For CFD data resolution is extremely high, making it simple to select the center plane accurately. The 200 mm field of view used in MR data acquisition allowed a selection of the center plane from these data sets with sub-millimeter accuracy. Likewise PIV affords the experimenter high-precision control over the laser sheet that defines the plane of data acquisition well into the sub-millimeter domain. Given these facts, it is reasonable to conclude that the respective center planes do come from similar enough locations within the model to make the data presented here significant.

5 Discussion

In addition to power loss estimation, there are a variety of other applications for which reconstructed velocity data would be well suited. Many vascular pathologies such as polycystic kidney disease (PKD) are characterized by decreased arterial blood flow [27]. The evaluation of disease progression in PKD cases is often based on in vivo flow measurements from MRI. For diagnoses to be accurate based on traditional two-dimensional images, it is important that sampling take place at precise locations. Reconstructed velocity data offers a complete flow field from which more global information is available. Accordingly, reconstructions could provide physicians with more information for diagnoses.

Fluid dynamics within the carotid artery are evaluated with ultrasound over 10,000 times each day in the U.S., with the aim of identifying plaque regions via the observation of flow [26]. However, the dimensionally limited and relatively low resolution data provided by ultrasound, coupled with its high operator dependency, result in operations that are unnecessarily performed 24% of the time [26]. MR reconstruction would be well-suited to improve analysis and diagnosis in this scenario because of the more complete description of three-dimensional in vivo fluid dynamics that it provides.

Another application in which reconstructed velocity data could be useful is the quantification of shear stress at vessel walls. Shear stress is known to play a role in atherosclerosis and other vascular pathologies. As comprehensive in vivo data are required for quantification, reconstructed velocity fields would offer a non-invasive alternative acquisition method to provide the necessary information. Given that reconstructed velocity data can be obtained for any number of different phases within the cardiac cycle, the oscillatory shear stress index could also be calculated in vivo.

Although the reconstruction of MRI velocity images has been the focus of research thus far, the ACGI methodology is also well suited for application to velocity data acquired via other means. The PIV data that have been discussed in this paper represent a valuable source of in vitro velocity information but provide only two-dimensional spatial samples of two-dimensional velocity vectors. ACGI could be used to enhance the out of plane resolution of standard two-dimensional PIV data sets, and to reconstruct three-dimensional data sets of three-dimensional velocity vectors given the availability of PIV data from multiple perspectives. Both of these options will be investigated in future research.

Regardless of future applications, the validations presented here have demonstrated that ACGI is capable of reconstructing detailed, high quality velocity data. This methodology has an inherent advantage over techniques that simply place acquired planes of velocity data into a common three-dimensional space because it takes an intelligent approach to the approximation of unacquired data. Other techniques for accomplishing this, including linear, cubic, and sinc function interpolation, suffer because interpolation is carried out between points that are unrelated with respect to the fluid structures to which they belong. In comparison to native methods of obtaining three-dimensional fields of three-dimensional velocity vectors, such as volumetric MR imaging, reconstruction requires substantially less acquisition time making it practical for a variety of clinical applications that volumetric acquisition techniques cannot address.

6 Conclusions

Qualitatively, reconstructed MR velocity fields displayed similar flow characteristics in comparison to both PIV and CFD. More insight into the quality of reconstruction was provided by a quantitative comparison. For both 2 L/min and 4 L/min total flow rates, errors between CFD and reconstructed MR velocity data were lower than errors between either CFD and PIV or MR reconstruction and PIV. This may indicate that the CFD and reconstructed velocity fields are more similar to each other than either is to PIV. The absolute evaluations of any one of these modalities are prohibited by the fact that a gold standard is unavailable. It is for this

reason that the divergence errors were examined and that comparison-based methods were used in this work. Results from both analyses indicate that velocity fields reconstructed from MR with the proposed ACGI technique are comparable in quality to those from the other data sources examined here.

Considering that MR reconstruction is the only one of these modalities capable of directly capturing in vivo information, the results support that the acquisition of complex three-dimensional in vivo velocity fields may now be possible. The implications of this would be widespread, but in the context of this work such velocity fields could be used to provide in vivo power loss estimations from the TCPC using the viscous dissipation function. An exploration of this prospect is underway and is one focus of ongoing research. This methodology is envisioned as an integral part of the surgical evaluation tool currently in development.

The development effort is based upon a number of fluid dynamic evaluation techniques including CFD, PIV, MR reconstruction, flow visualization, studies in theory, and experimental studies like those conducted by Sharma et al. Through the use of all these varied techniques with their respective strengths and weaknesses, the identification of the elusive gold standard in fluid dynamic data acquisition becomes more feasible. Moreover, each of these tools contributes to a system of checks and balances that validates and ensures the effective use of every other tool, the ultimate goal being a comprehensive system capable of providing physicians with accurate and clinically valuable in vivo fluid dynamic data.

The proposed ACGI algorithm performs well in the velocity reconstruction application, as the validations indicate. Through its exploitation of both gradient and intensity information, ACGI is adept at reconstructing data near boundaries. This point is especially significant in the velocity data context as accurate values near boundaries are imperative when reconstructions are to be used for power loss estimation via the viscous dissipation function. Fluid dynamic theory and both in vitro and in vivo observations indicate that the highest magnitude velocity gradients are found near fluid boundaries. These gradients are the largest contributors to the power loss values estimated with the dissipation function. Accordingly, the characteristics of ACGI make the proposed algorithm well suited for the reconstruction of data to be used with the viscous dissipation function, and in virtually any other application requiring high-quality three-dimensional velocity information from MR.

The viscous dissipation function has been investigated previously, and data supporting its accuracy in estimating power loss were presented in Section 1. Combining the velocity reconstruction technique proposed here with the viscous dissipation function provides the first established methodology for noninvasively estimating power loss based completely on in vivo data. Within this framework, the application of ACGI to velocity field reconstruction creates a valuable tool for the evaluation of executed operations, aimed ultimately at producing successful surgical outcomes.

Acknowledgment

This work was supported by a grant from the National Institutes of Health—NHLBI (R01HL67622). The Children's Hospital of Philadelphia, Egleston Children's Hospital, Emory University, and the University of North Carolina at Chapel Hill have also contributed significantly to this research.

References

[1] Migliavacca, F., Kilner, P., Pennati, G., Dubini, G., Pietrabissa, R., Fumero, R., and de Leval, M., 1999, ''Computational Fluid Dynamic and Magnetic Resonance Analyses of Flow Distribution Between the Lungs After Total Cavopulmonary Connection,'' IEEE Trans. Biomed. Eng., **46**, pp. 393–399.
[2] Bolzon, G., Pedrizzetti, G., Grigioni, M., Zovatto, L., Daniele, C., and D'Avenio, G., 2002, ''Flow on the Symmetry Plane of a Total Cavo-Pulmonary Connection,'' J. Biomech., **35**, pp. 595–608.
[3] de Leval, M. R., Dubini, G., Migliavacca, F., Jalali, H., Camporini, G., Redington, A., and Pietrabissa, R., 1996, ''Use of Computational Fluid Dynamics in the Design of Surgical Procedures: Application to the Study of Competitive Flows in Cavopulmonary Connections,'' J. Thorac. Cardiovasc. Surg., **111**, pp. 502–513.
[4] Amodeo, A., Grigioni, M., Oppido, P., Daniele, C., D'Avenio, G., Pedrizzetti, G., Giannico, S., Filippelli, S., and Di Donato, R. M., 2002, ''The Beneficial Vortex and Best Spatial Arrangement in Total Extracardiac Cavopulmonary Connection,'' Surg. For Congenital Heart Disease, **124**, pp. 471–478.
[5] Saber, N. R., Gosman, A. D., Wood, N. B., Kilner, P. J., Charrier, C. L., and Firmin, D. N., 2001, ''Computational Flow Modeling of the Left Ventricle Based on In Vivo MRI Data: Initial Experience,'' Ann. Biomed. Eng., **29**, pp. 275–283.
[6] Lee, T., and Wang, W., 2000, ''Morphology-Based Three-Dimensional Interpolation,'' IEEE Trans. Med. Imaging, **19**, pp. 711–721.
[7] Higgins, W. E., Morice, C., and Ritman, E. L., 1993, ''Shape-Based Interpolation of Tree-Like Structures in Three-Dimensional Images,'' IEEE Trans. Med. Imaging, **12**, pp. 439–450.
[8] Treede, G. M., Prager, R. W., Gee, A. H., and Berman, L., 2000, ''Surface Interpolation From Sparse Cross Sections Using Region Correspondence,'' IEEE Trans. Med. Imaging, **19**, pp. 1106–1114.
[9] Grevera, G. J., and Udupa, J. K., 1996, ''Shape-Based Interpolation of Multidimensional Gray-Level Images,'' IEEE Trans. Med. Imaging, **15**, pp. 881–892.
[10] Raya, S. P., and Udupa, J. K., 1990, ''Surface Shape-Based Interpolation of Multidimensional Objects,'' IEEE Trans. Med. Imaging, **9**, pp. 32–42.
[11] Grevera, G. J., and Udupa, J. K., 1998, ''An Objective Comparison of 3-d Image Interpolation Methods,'' IEEE Trans. Med. Imaging, **17**, pp. 642–652.
[12] Reller, M., McDonald, R., Gerlis, L., and Thornburg, K., 1991, ''Cardiac Embryology: Basic Review and Clinical Correlations,'' J. Am. Soc. Echocardiogr, **4**, pp. 519–532.
[13] Schlichting, H., 1979, *Boundary Layer Theory*, McGraw-Hill, New York.
[14] Migliavacca, F., Dubini, G., Pennati, G., Pietrabissa, R., Fumero, R., Hsia, T., and de Leval, M. R., 2000, ''Computational Model of the Fluid Dynamics in Systemic-to-Pulmonary Shunts,'' J. Biomech., **33**, pp. 549–557.
[15] Spicer, C. A., and Taylor, C. A., 2000, ''Simulation-Based Medical Planning for Cardiovascular Disease: Visualization System Foundations,'' Comput. Aided Surg., **2**, pp. 82–89.
[16] Healy, T. M., Lucas, C., and Yoganathan, A. P., 2001, ''Non-Invasive Fluid Dynamic Power Loss Assessments for Total Cavopulmonary Connections Using the Viscous Dissipation Function: A Feasibility Study,'' ASME J. Biomech. Eng., **123**, pp. 317–324.
[17] Sharma, S., Goudy, S., Walker, P., Panchal, S., Ensley, A., Kanter, K., Tam, V., Fyfe, D., and Yoganathan, A., 1996, ''In Vitro Flow Experiments for Determination of Optimal Geometry of Total Cavopulmonary Connection for Surgical Repair of Children With Functional Single Ventricle,'' J. Am. Coll. Cardiol., **27**, pp. 1264–1269.
[18] Ensley, A., 2000, ''A Fluid Mechanic Assessment of the Total Cavopulmonary Connection,'' Masters thesis, Georgia Institute of Technology.
[19] Monaco, J., 1997, ''Motion Models for Video Applications,'' Ph.D. thesis, Georgia Institute of Technology.
[20] Horn, B., 1968, *Robot Vision*, The MIT Press, pp. 280–292.
[21] Frakes, D., Sinotte, C. M., Conrad, C. P., Healy, T. M., Shiva, S., Fogel, M. A., Monaco, J. W., Smith, M. J., and Yoganathan, A., 2002, ''Application of an Adaptive Control Grid Interpolation Technique to Morphological Vascular Reconstruction,'' Proc. SPIE Int. Soc. Opt. Eng., **4684**, pp. 1161–1167.
[22] Shung, K., Smith, M., and Tsui, B., 1992, *Principles of Medical Imaging*, Academic Press, San Diego, pp. 213–267.
[23] Ensley, A. E., Ramuzat, A., Healy, T. M., Chatzimavroudis, G. P., Lucas, C., Sharma, S., Pettigrew, R., and Yoganathan, A. P., 2000, ''Assessment of the Fluid Mechanics of the Total Cavopulmonary Connection Using Magnetic Resonance Phase Velocity Mapping and Digital Particle Image Velocimetry,'' Ann. Biomed. Eng., **28**, pp. 1172–1183.
[24] Dubini, G., de Leval, M. R., Pietrabissa, R., Montevecchi, F. M., and Fumero, R., 1996, ''A Numerical Fluid Mechanical Study of Repaired Congenital Heart Defects: Application to the Total Cavopulmonary Connection,'' J. Biomech., **29**, pp. 111–121.
[25] Frakes, D., Monaco, J., and Smith, M., 2001, ''Suppression of Atmospheric Turbulence in Video Using an Adaptive Control Grid Interpolation Approach,'' in *Proceedings of the International Conference on Acoustics, Speech, and Signal Processing*.
[26] Ferraro, F., 2003, *Quantum Medical Radiology*, personal interview.
[27] Wallin, A., Frakes, D., Brummer, M. E., Yoganathan, A., and Chapman, A. B., 2003, ''Improvements in Validation Studies: Polyvinyl Alcohol (PVA) Phantoms and Magnetic Resonance Imaging,'' in *Proceedings IEEE Biomedical Engineering Society Annual Fall Meeting*.